Blockage Corrections for Tidal Turbines-Application to an Array of Turbines in the Alderney Race

Nasteho Djama Dirieh, Jérôme Thiébot, Sylvain Sébastien Guillou, Nicolas Guillou

energies

MDPI

Article

Blockage Corrections for Tidal Turbines—Application to an Array of Turbines in the Alderney Race

Nasteho Djama Dirieh [1], Jérôme Thiébot [1,*], Sylvain Guillou [1] and Nicolas Guillou [2]

[1] LUSAC, UNICAEN, Normandie Université, 60 Rue Max Pol Fouchet, CS 20082, 50130 Cherbourg en Cotentin, France; nasteho.djama-dirieh@unicaen.fr (N.D.D.); sylvain.guillou@unicaen.fr (S.G.)
[2] Laboratoire de Génie Côtier et Environnement, ER, Cerema, 155 Rue Pierre Bouguer, Technopôle Brest-Iroise, BP 5, 29280 Plouzane, France; nicolas.guillou@cerema.fr
* Correspondence: jerome.thiebot@unicaen.fr

Abstract: Tidal turbines are located in shallow water depths in comparison to their dimensions (15 m-diameter turbines in 40 m depths, typically). Constrained vertically by the water depth and laterally by neighbouring turbines, the flow within a tidal farm is subjected to blockage effects that influence the performance of individual devices. The Betz limit (which is the maximum power extractable from an unconstrained flow) can, therefore, be exceeded as demonstrated by Garrett and Cummins. Thus, beyond a significant blockage ratio, blockage effects should be considered when assessing the energy production of a tidal farm. The actuator disk method is particularly suited to simulate the flow field within an array of turbines under realistic tidal flow conditions. However, the implementation of actuator disks in coastal numerical models relies on relationships that neglect the blockage effects on the thrust and power of devices. We propose here an actuator disk formulation corrected to integrate these effects. This modified formulation, based on the model of Whelan et al., is integrated into a regional implementation of a three-dimensional model Telemac3D targeted towards the Alderney Race (English Channel). The method is applied to two hypothetical tidal farms with aligned and staggered arrangements, respectively. Blockage corrections of the thrust and power coefficients are found to have counterbalanced effects on the array production. Thrust correction results in a noticeable flow reduction within the array. However, the associated decrease of the array production is counterbalanced by the increase of the turbine power coefficient. Blockage corrections were, therefore, found to result in a slight increase, by 3%, of the array production over a mean spring tidal cycle.

Keywords: tidal turbine; actuator disk; blockage; Telemac3D; Alderney Race

Citation: Djama Dirieh, N.; Thiébot, J.; Guillou, S.; Guillou, N. Blockage Corrections for Tidal Turbines—Application to an Array of Turbines in the Alderney Race. *Energies* **2022**, *15*, 3475. https://doi.org/10.3390/en15103475

Academic Editor: Madjid Karimirad

Received: 19 April 2022
Accepted: 5 May 2022
Published: 10 May 2022

1. Introduction

Over the last few decades, interest in the exploitation of renewable energy sources has increased in response to the impacts of global warming. With the second largest maritime area in the world (11 millions of km^2), France has the capacity to increase its exploitation of marine energy resources (offshore wind, tide, wave, thermal and osmotic gradients…). The Alderney Race, located in the English Channel between the Alderney Island and the Cap de la Hague (France), is one of the most promising tidal-stream energy sites in the world, capitalising almost half of the total French tidal resources [1]. The high energy potential of the Alderney Race, thus, attracts industrial projects. For instance, Simec Atlantis and HydroQuest plan to test tidal turbines on-site in the next few years, which will be a first step towards larger projects.

In 2022, existing tidal farms contain few devices (less than four). Thus, knowledge on the flow interactions between turbines and on the design of arrays are limited. Furthermore, there are few observations available on the wakes of turbines deployed in real sea-conditions. The design of future tidal farms, thus, relies mostly on scaled laboratory experiments, analytical and numerical models [2–5].

Regarding numerical approaches, a simple method to represent a tidal array is named the "bed friction approach". It consists of applying a force equivalent to the global effect of turbines in the area occupied by the tidal farm. The force (thrust and drag) is included in the momentum equations with a formulation similar to a bed friction term (a sink term depending on the squared velocity magnitude). As the turbines are not represented individually but as a whole, the flow interactions between turbines cannot be captured [6]. Thus, this technique is generally retained in two-dimensional regional studies [7] to assess the far-field effects of tidal farms on sediment dynamics [8] or hydrodynamics [9]. The "line momentum sink" approach is another way to simulate the effects of tidal arrays in coastal flow models. This approach consists of using a discontinuity line to represent the head loss across one or several fence(s) of turbines. The head loss is calculated from the Bernoulli equation and the momentum equations following the theoretical model of Houlsby et al. [10]. Applications can be found in [11–13]. Although discontinuity lines simulate the energy extraction along fences of turbines, the flow is not resolved at the turbine scale and the interactions between devices are, therefore, highly simplified (as the turbine effect is uniform along the line(s)). This method is, therefore, also more suitable for regional studies than for wake-field studies.

The Actuator Disk (AD) concept is a simplified method to investigate the hydrodynamics interactions of horizontal axis tidal turbines. It consists of representing the energy extraction by momentum sink terms applied in the areas swept by turbines blades. Although the AD concept neglects the swirl and the turbulent processes, especially the vortexes shed by the blades, it has been validated with various laboratory data and has proven its ability to approach the flow dynamics in the far wake(s) of individual or multiple tidal turbine(s) [3,14–17]. In contrast to more sophisticated methods, such as blade element momentum theory or blade-resolved models, the AD approach can be implemented in regional models. Hence, associating ADs with coastal flow models enables both the simulation (1) of realistic tidal flow conditions and (2) flow interactions between turbines. These advanced simulations are required to optimise the layout of turbines and to assess the annual energy production of a proposed array. There are several examples of near- and far-field studies performed with ADs [3,15,18–21]. For instance, Roc et al. [3] and Michelet et al. [19] integrated ADs in the three-dimensional (3D) model Regional Ocean Modelling System (ROMS). Michelet et al. [19] investigated the impact of the tidal asymmetry on the power output for two configurations of eight turbines in the Fromveur Strait (western Brittany, France). A comparable application relying on a Fluent model was carried out by Nguyen et al. [20] who highlighted the influence of current misalignment on the energy production of an array in the Alderney Race. More recently, Thiébot et al. [18] complemented this wake field study by relying on a modified version of Telemac3D implemented in the Alderney Race. This investigation exhibited especially the great influence of the wake-induced turbulence on the flow recovery in the turbines wakes. Abolghasemi et al. [21] also retained ADs, implemented in the Fluidity solver, to simulate flow interactions between turbines and to optimise the positioning of an array of 32 turbines.

Tidal turbines are deployed in shallow depths (depths ranging between 30 and 60 m for turbines of 10 to 20 m diameter, typically). As the flow is constrained vertically and laterally, the performance of turbines differs from what would be obtained in an unbounded flow. Experimental studies demonstrated that (1) the influence of blockage becomes significant when the blockage ratio B, which is defined as the ratio of the rotor swept area to the cross-sectional area of the flow, exceeds a value of 5–10% [22] and that (2) high blockage ratios lead to an increase of the flow velocities through and around the rotor, which both increases torque (and hence power) and thrust of turbine [23–26]. The Betz limit, which characterizes the maximum amount of energy (or power) that can be extracted from a turbine in an unconfined flow, can thus be exceeded. By applying Betz's theory to a constrained flow, Garrett and Cummins [27] showed that the Betz limit is proportional to $(1 - B)^{-2}$. The calculation of the efficiency of a tidal turbine farm should, therefore, consider blockage effects, in particular the change of the thrust and power coefficients as a function

of the blockage ratio. The change of these coefficients is here referred to as "blockage correction". These corrections can be given by analytical models [27–30]. Among these analytical models, the model of Nishino and Willden [29] permits assessing the efficiency of a turbine array partially blocking a cross-section of a tidal channel. It relies on the model of Garrett and Cummins [27], which is applied at two scales. (1) The "global" scale permits to investigate the flow through and around the array and (2) at the "local" scale permits to study the flow through and around each turbine. The model uses two different types of blockage ratios, referred as "local" and "global". A local blockage is defined as the ratio between the surface area of a turbine and the cross-sectional area of the local flow passage (Equation (1)). A global blockage is defined as the ratio of the area swept by all turbines to the cross-sectional area of the channel (Equation (2)) (Figure 1). In an infinitely wide channel and for a small turbine array (the global blockage tending to zero), this two-scale model resulted in the maximum energy extraction for a local blockage ratio of 0.4. In this case, the maximum power coefficient C_P reached 0.80 [29] or 0.89 [30], depending if the head loss induced by the turbines is considered or not. Finally, the effects of blockage on thrust and power of tidal turbines have also been investigated numerically [24,24,25,31,32]. For instance, Nishino and Willden [24] investigated idealised flow conditions around a single turbine, and Thiébot et al. [33] analysed the efficiency (expressed in terms of the thrust and power coefficients) of fences of tidal turbines deployed in the Alderney Race.

$$B_L = \frac{\pi d^2/4}{h(d+s)}. \tag{1}$$

where h is the water depth, d is the turbine diameter, s is the intra-turbine spacing and $(d+s)$ is the centre-to-centre distance between neighbouring turbines.

$$B_G = \frac{n\pi d^2/4}{lh}. \tag{2}$$

where n is the number of turbines.

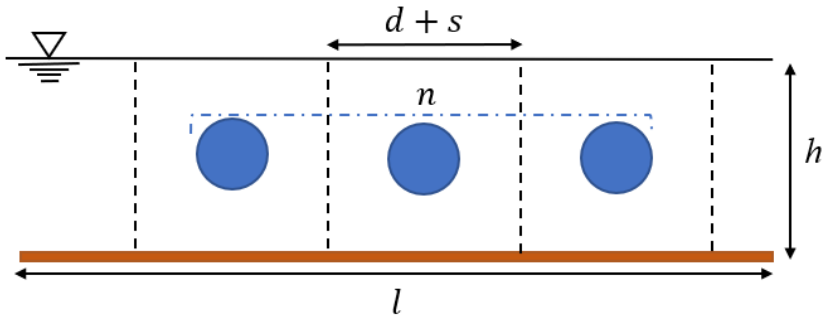

Figure 1. Cross-sectional view of the channel.

In numerical wake-field studies relying on ADs, the turbines thrust (hence, the momentum sink terms) are computed from the thrust coefficients and squared current velocity magnitudes. Rigorously, the thrust should integrate corrections to consider the blockage effect. However, in most applications, corrections are neglected [3,18], which is acceptable only when B is small (smaller than 5–10%, typically). In the present investigation, we integrate blockage corrections for the thrust and the power coefficients and assess the influence of the corrections by considering two hypothetical configurations of tidal farms in the Alderney Race with aligned and staggered layouts. The corrections are computed from the analytical model of Whelan et al. [28], which derives from the reference model of Garrett and Cummins [27] and integrates, in addition, the variation of water depth above the turbine(s).

The paper is organised as follows: Section 2 is dedicated to the description of the study site (Section 2.1), the analytical model of Whelan et al. [28] (Section 2.2) and the numerical

model in which we implemented an AD formulation with blockage corrections (Section 2.3). The results are presented and discussed in Section 3. Section 4 contains our conclusions.

2. Materials and Method

2.1. Study Site and Turbine Array

The Alderney Race is the site selected for this study. It is a strait with a width of 15 km located in the English Channel, between the Cap de la Hague and Alderney Island. With maximum current speeds exceeding 5 m/s during spring tides and depths suitable for deploying tidal turbines, it is one of the most promising tidal stream energy sites in the world. Several resource assessments have been conducted to estimate the potential energy production of this site [1,34–39]. The potential power technically exploitable in the Alderney Race is 1.7 GW [34]. Several wake-field studies have been performed on this site relying either on AD [4,18,20] or analytical wake models [40].

The scenarios of tidal energy extraction considered in this study are taken from [18]. The computational domain covers the English Channel (Figure 2) in order to achieve suitable open boundary conditions and, therefore, reliable current predictions in the area covered by the tidal array. In the Alderney Race, the mesh size is of the order of 100 m and decreases to 1 m within the tidal farm. The zone of refined mesh is 2000 m long and 500 m wide, with a mean water depth of 44 m and limited change of bathymetry (smaller than 1 m over the study zone). Further details can be found in [18]. Two layouts are considered and rely on either aligned or staggered arrangements keeping the same number of rows and nearly the same number of devices per row. Thus, the first configuration contains 30 turbines aligned with a lateral inter-turbine spacing of 3 diameters (D) and an inter-row spacing of 5D. The second configuration contains 28 staggered turbines with a lateral inter-turbine spacing of 3D and an inter-row spacing of 5D (Figure 3). To be consistent with [18], the turbine diameter is 14 m. Computations are performed to simulate a mean spring tide that occurred on 9 August 2014.

2.2. Analytical Model

The Linear Momentum Actuator Disk Theory (LMADT) permits estimation of the performance of a turbine (thrust and power) for an idealised flow. This theory relies on the conservation of mass, momentum and energy through and around a turbine. In an unbounded flow, the LMADT leads to the Betz limit, which implies that the maximum power coefficient (i.e., the maximum portion of power that can be extracted from the flow) is 0.59. This limit is reached when the velocity downstream of the disc is equal to one third of the upstream velocity magnitude. Regarding tidal turbines, blockage effects have a significant impact on the performance of turbines. Different analytical models, based on LMADT, have therefore been developed for this type of application. The model of Whelan et al. [28] is used here to obtain expressions for the blockage corrections. It relies on the LMADT and is obtained by considering the flow in a vertical plane, as represented in Figure 4. This model derives from the reference model of Garrett and Cummins [27] and integrates the effect of the change of water depth above the turbine (Figure 4). The model of Whelan et al. [28] relies on a bidimensional (2D) analysis where the turbine area is distributed over an unit width. The blockage ratio, which is classically defined as the ratio of the blade swept area to the cross-sectional area $B = \left(\frac{\pi r^2}{lh}\right)$, therefore, becomes: $B = \frac{s_d}{h}$, where the equivalent diameter is s_d. The flow velocity in the disc is denoted $U_d = \beta U_\infty$. The velocity outside the stream tube, far downstream is $U_2 = \gamma U_\infty$. At a certain distance behind the disc, it is assumed to be uniform along the vertical.

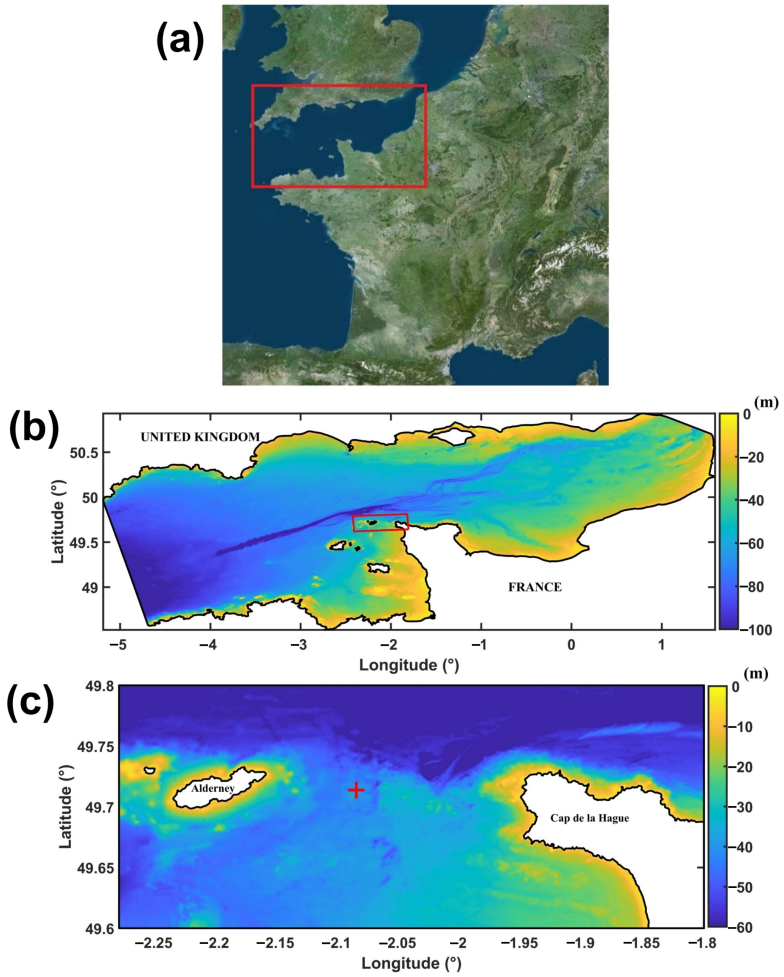

Figure 2. (**a**) Location of the study zone. (**b**) English Channel computational domain and bathymetry. (**c**) The red cross represents the location of the array.

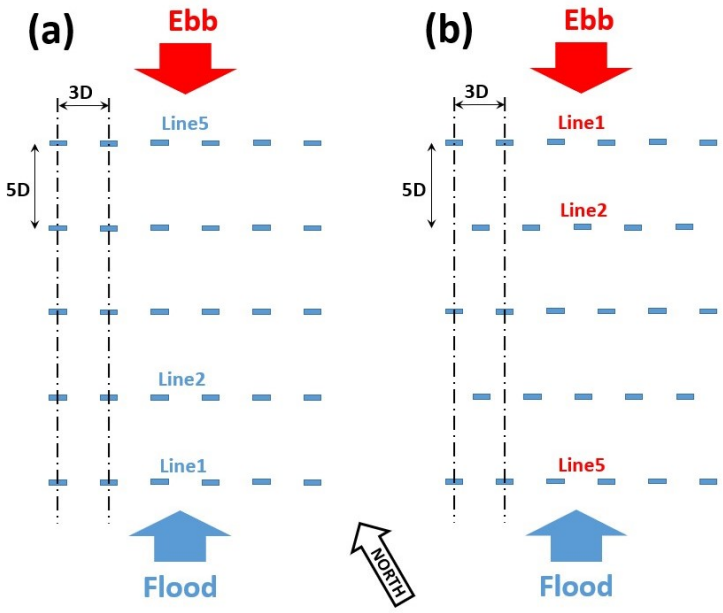

Figure 3. Schematic representation of the two configurations. (**a**) Aligned layout and (**b**) staggered layout. The rows are numbered in the direction of the flow. Thus, line 1 stands for the row located in the free stream.

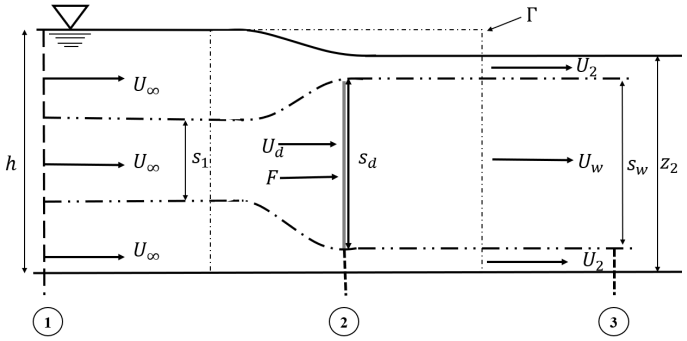

Figure 4. Schematic representation of the flow around an AD in a channel with free surface deformation. The numbers 1–3 represent particular locations (upstream, at the disk, downstream).

The main assumptions and equations are outlined below using the notations shown in Figure 4 where three locations are identified. The variables are listed in Abbreviations. Location (1) is far enough upstream of the turbine that the pressure and velocity can be considered uniform. Location (2) corresponds to the turbine. The location (3) is far enough downstream that the pressure can be considered uniform. The "core flow" is the stream passing through the turbine, and the "bypass flow" is the flow that circumvents the turbine. At location (3), the core flow velocity is denoted $U_w = \alpha U_\infty$ (where α represents the velocity reduction in the far wake). The turbine velocity is denoted $U_d = \beta U_\infty$ (where β represents the velocity reduction at the location of the turbine). At a certain distance behind the disc, the bypass flow velocity is assumed to be uniform along the vertical and is denoted $U_2 = \gamma U_\infty$ (where γ is the change in velocity in the bypass wake).

The continuity equation in the bypass flow is:

$$U_\infty(h - s_1) = \gamma U_\infty(z_2 - s_w). \tag{3}$$

Applying continuity in the stream tube gives:

$$U_\infty s_1 = \beta U_\infty s_d = \alpha U_\infty s_w. \tag{4}$$

Equations (3) and (4) give:

$$\beta = \frac{\alpha}{B(\gamma - \alpha)}\left[\gamma\left(1 - \frac{\delta z}{h}\right) - 1\right], \tag{5}$$

where $\delta z = h - z_2$ represents the change in free surface elevation, which is given by the Bernoulli equation applied between the inlet and outlet of the channel:

$$\frac{\delta z}{h} = \frac{Fr^2}{2}\left(\gamma^2 - 1\right) \tag{6}$$

where Fr is the Froude number defined as the ratio between potential and inertia forces in a free surface flow: $Fr = \frac{U_\infty}{\sqrt{gh}}$, where g is the acceleration of the earth's gravity.

Neglecting the pressure drop between the upstream and the downstream regions of the disc, the Bernoulli equation applied along the longitudinal axis of the disc gives an expression of the thrust exerted by the turbine:

$$F = s_d \delta p = \rho s_d\left[g\delta z + \frac{1}{2}U_\infty^2\left(1 - \alpha^2\right)\right]. \tag{7}$$

This force can also be obtained using the integrated momentum balance (Euler equation) over the volume Γ (Figure 4):

$$F = \frac{1}{2}\rho g\left(2h\delta z - (\delta z)^2\right) + \rho U_\infty^2 h(1 - \gamma) + \rho\beta U_\infty^2 s_d(\gamma - \alpha). \tag{8}$$

The conservation of mass (Equation (3)), the Bernoulli equation (Equation (7)) and the integrated momentum equation (Equation (8)) yield a quartic polynomial depending on Fr, B, α and γ (Equation (9)). In this polynomial, the unknowns are α and γ. Fr and B depend on the flow conditions and the dimensions of the turbine.

$$\begin{aligned} &Fr^2\gamma^4 + 4\alpha Fr^2\gamma^3 + \left(4B - 4 - 2Fr^2\right)\gamma^2 \\ &+\left(8 - 8\alpha - 4Fr^2\alpha\right)\gamma + \left(8\alpha - 4 + Fr^2 - 4\alpha^2 B\right) = 0. \end{aligned} \tag{9}$$

The solution of the quartic polynomial is limited to the physical solution of the bypass flow. Solving this polynomial gives an expression of γ (bypass induction factor). Thus, it is possible to calculate the axial induction factor a (Equation (10)), the thrust coefficient C_T (Equation (11)) and the power coefficient C_P (Equation ((12)).

$$a(B) = 1 - \frac{U_d}{U_\infty}(B) = 1 - \beta(B). \tag{10}$$

$$C_T(B) = \left(\gamma(B)^2 - \alpha(B)^2\right). \tag{11}$$

$$C_P(B) = \beta(B)C_T(B) \tag{12}$$

The effect of the blockage on the thrust coefficient is illustrated in Section 2.3. In the following, blockage effects are accounted for when both (1) computing the thrust of the turbines implemented in the regional model (hence, the momentum sink terms) and (2) assessing the turbine output.

2.3. Numerical Model

Telemac3D [41] is a hydrodynamic model of free surface environmental flows. It relies on the finite element method and solves the unsteady RANS equations. The continuity and momentum equations are:

$$\frac{\partial u}{\partial x} + \frac{\partial v}{\partial y} + \frac{\partial w}{\partial z} = 0 \tag{13}$$

$$\begin{cases} \dfrac{\partial u}{\partial t} + u\dfrac{\partial u}{\partial x} + v\dfrac{\partial u}{\partial y} + w\dfrac{\partial u}{\partial z} = -\dfrac{1}{\rho}\dfrac{\partial p}{\partial x} + \nu_{eff}\Delta u + S_x \\ \dfrac{\partial v}{\partial t} + u\dfrac{\partial v}{\partial x} + v\dfrac{\partial v}{\partial y} + w\dfrac{\partial v}{\partial z} = -\dfrac{1}{\rho}\dfrac{\partial p}{\partial y} + \nu_{eff}\Delta v + S_y \\ \dfrac{\partial w}{\partial t} + u\dfrac{\partial w}{\partial x} + v\dfrac{\partial w}{\partial y} + w\dfrac{\partial w}{\partial z} = -\dfrac{1}{\rho}\dfrac{\partial p}{\partial z} + g + \nu_{eff}\Delta w + S_z \end{cases} \tag{14}$$

where x and y are the horizontal coordinates; z is the vertical coordinate; S_x, S_y and S_z are the source and sink terms (the external forces acting on the fluid in the present investigation); t is the time; u, v and w are the three components of the velocity; p is the pressure; ν_{eff} is the effective kinematic viscosity of the fluid (the sum of the viscosity of the fluid and the turbulent viscosity computed with the turbulence closure); and ρ is the density of the fluid, which is assumed to be constant and equal to 1025 kg·m^{-3} here.

In earlier studies, ADs have been implemented in Telemac3D with the momentum sink terms [4,39]:

$$\overrightarrow{S} = -\frac{\overrightarrow{F}}{Ae} = -\frac{1}{2}\frac{K}{e}\overrightarrow{U_d}\|\overrightarrow{U_d}\|. \tag{15}$$

where e is the thickness of the disc and K is a resistance coefficient.

This formulation derives from the definition of the thrust (Equation (16)). Of note, numerous ADs are implemented using induction factor a rather than the resistance coefficient K. However, the correspondence between the two formulations can be found with Equation (17) [28].

$$\overrightarrow{F} = \frac{1}{2}\rho A C_T \overrightarrow{U_\infty}\|\overrightarrow{U_\infty}\|. \tag{16}$$

$$K = \frac{C_T}{(1-a)^2} \tag{17}$$

When running a numerical model with AD, it is important to consider what velocity to use for computing the sink term. Using the thrust definition (Equation (16)) requires determining the upstream velocity U_∞, which is not trivial because there is no undeniable method to determine the unperturbed flow characteristics, especially within a tidal farm where multiple wakes overlap. Furthermore, the use of a non-local velocity is not desirable from a computational point of view [42]. To circumvent this problem, the thrust introduced in an AD is often calculated from a local velocity (velocity in the disc) U_d (as in Equation (15)) and a relationship, such as the formulation proposed by Taylor [43], which uses a resistance coefficient K (Equation (18)). Of note, the two formulations of thrust (relying either on local or upstream velocities) are related with Equation (19).

$$U_\infty = U_d(1 + 0.25K) \tag{18}$$

$$C_T = \frac{K}{(1+0.25K)^2} \tag{19}$$

Rigorously, the aforementioned formulations are valid for an unbounded flow. In practice, they remain applicable for configurations with low blockage ratio (B smaller than 5–10%, typically) [3,19,20]. However, for more constrained flows, corrections should be applied. Thus, we propose here to include corrections and to assess their influence by comparing simulations with and without blockage corrections. Figure 5 represents the overall methodology.

For simulations without corrections (the left side of Figure 5), we chose a thrust coefficient $C_T = 0.8$ [44]. This value corresponds to a resistance coefficient $K = 1.528$ (Equation (19)) and to an induction factor $a = 0.276$. The value of K is included in Telemac3D to compute the momentum sink term according to Equation (15). Once the computation is achieved, the power output is assessed by integrating over the disks the cubed velocity magnitude, considering a constant value of $K(= 1.528)$. For a given turbine (numbered i), the extracted power is obtained with Equation (22), where $U_{d_{ij}}$ is the velocity in the disc and N is the number of nodes contained in the AD (nodes are numbered with index j). The mean production of the turbines deployed in the array is evaluated with Equation (23).

For the simulations with blockage corrections (the middle and right side of Figure 5), the thrust coefficient is modified according to the model of Whelan et al. [28] (Section 2.2). The correction depends on the ambient flow conditions (U_∞, h, Fr, B), which are computed from a preliminary simulation without turbines (Section 3). For instance, under certain flow conditions (e.g., $Fr = 0.152$ and $B = 0.09$), the correction increases and reaches $C_T = 0.932$ as illustrated in Figure 6, which shows the evolution of the thrust coefficient as a function of the induction factor. As the thrust coefficient is corrected, the resistance coefficient increases and reaches for instance, under certain flow conditions ($Fr = 0.152$ and $B = 0.09$), $K = 1.780$ (according to Equation (20)). Therefore, when the effect of blockage correction is considered, the momentum sink term included in Telemac (Equation (21)) increases, which modifies the flow field (and hence the available power).

$$K(B) = \frac{C_T(B)}{\beta(B)^2} \tag{20}$$

$$\overrightarrow{S} = -\frac{1}{2}\frac{\left(\gamma(B)^2 - \alpha(B)^2\right)}{\beta^2 e}\overrightarrow{U_d}\|\overrightarrow{U_d}\|. \tag{21}$$

The blockage correction on the power is accounted for a posteriori, when assessing from a given flow field, the global and individual power extracted by the turbines. In Equations (22) and (23), we use the values of K (variable in time) given by the model

of Whelan et al. [28] (see Equation (20)). Of note, as the water depth and current magnitude are not constant in time (Section 3), K varies in time as shown in Figure 7.

$$P_i(t) = \frac{1}{N}\sum_{j=1}^{N}\frac{1}{2}\rho K(t) A U_{d_{ij}}(t)^3 \tag{22}$$

$$\overline{P(t)} = \frac{1}{n}\sum_{i=1}^{n} P_i(t) \tag{23}$$

where n is the number of devices in the array.

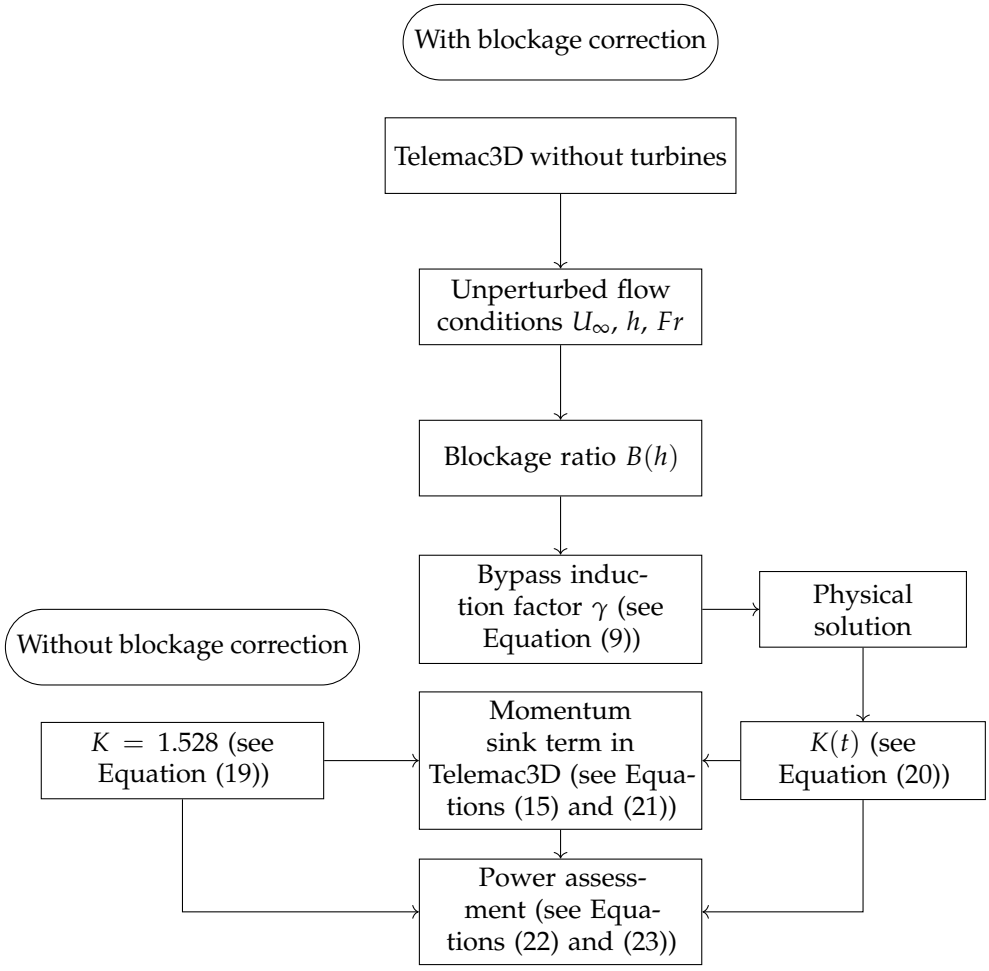

Figure 5. Methodology used in this study.

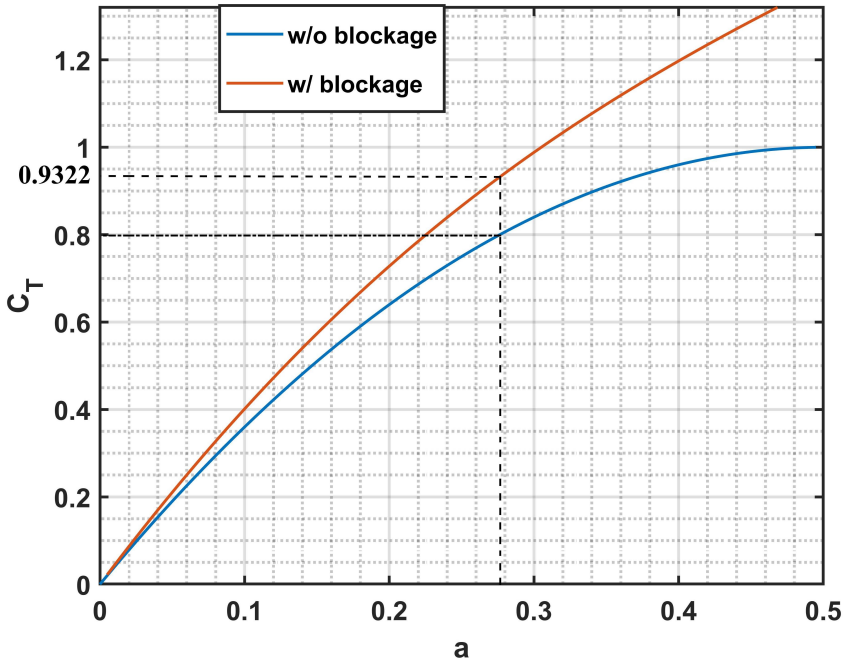

Figure 6. Evolution of the thrust coefficient as a function of the induction factor for the case with blockage correction (red curve) and for the case without blockage corrections (blue curve). The values of Fr and B are calculated from the averaged values of velocities and water depth retained for our application in the Alderney Race (Section 3, Table 1) ($Fr = 0.152$ and $B = 0.09$).

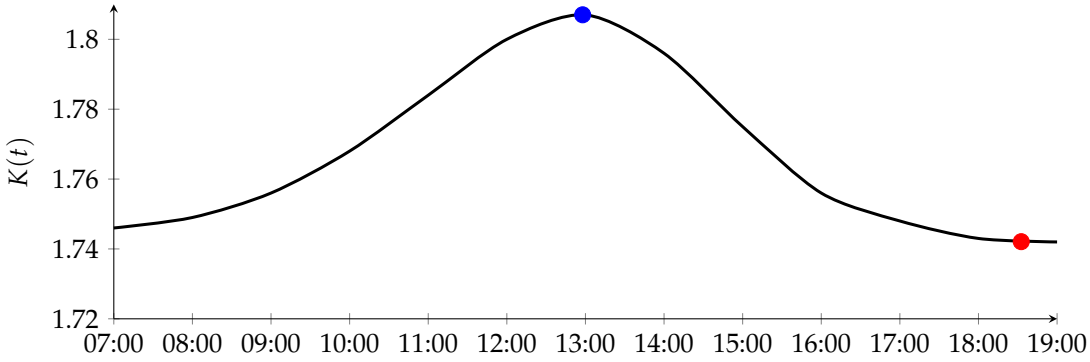

Figure 7. Time-series of the resistance coefficient K during a mean spring tide on 9 August 2014. The peak ebb and flood are represented by blue and red circles, respectively.

Table 1. Characteristics of the flow during peak ebb and flood in the centre of the tidal farm (49.705° N; 2.103° W).

	Peak Ebb	Peak Flood
Velocity magnitude (m/s)	3.02	2.76
Velocity direction (°/North)	206	32
Water depth (m)	41.05	46.52
Froude number (dimensionless)	0.150	0.129
Local blockage ratio (%)	8.93	7.88

3. Results and Discussion

The temporal evolution of velocities and free surface elevation extracted from the Telemac3D model in the centre of the tidal farm for a simulation without tidal turbines are shown in Figure 8. This figure shows that, at the location considered in the Alderney Race, we obtain the maximum velocity magnitude at low and high tides. The spatial

distribution of the velocities, for a simulation without tidal turbines, during (a) the peak ebb and (b) peak flood is shown in Figure 9. The characteristics of the flow at the peak flood and ebb are summarised in Table 1. The Froude number (defined in Section 2.2) varies with the water depth and the current magnitude. The local blockage ratio also depends on the water depth. It is 8.93% at peak ebb (high tide) and 7.88% at peak flood (low tide) (Table 1). Finally, the global blockage ratio is small (<1%) as the lateral dimensions of the tidal array (of the order of 200 m) are small in comparison to the width of the Alderney race (of the order of 15 km).

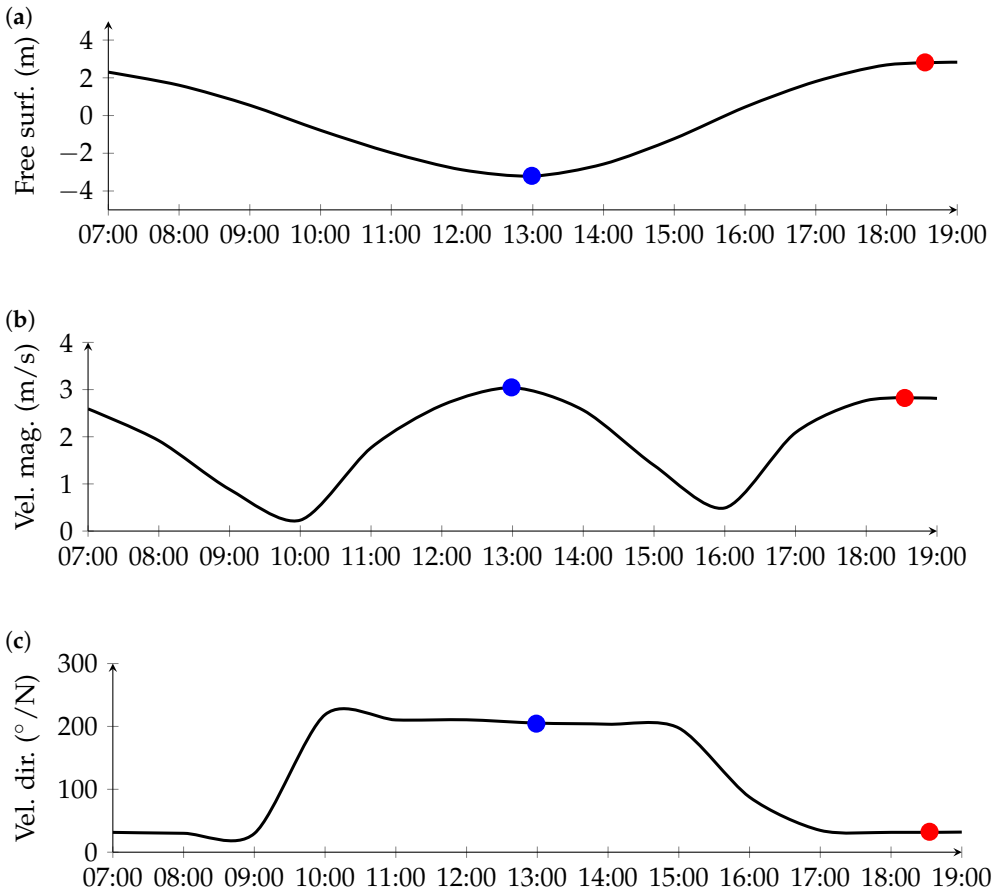

Figure 8. Time-series of (**a**) free surface elevation (with respect to the mean sea level), (**b**) depth-averaged velocity magnitude and (**c**) depth-averaged velocity direction (nautical convention) extracted from the Telemac3D model (simulation without turbines) in the centre of the tidal farm (49.705° N; 2.103° W) during a mean spring tide on 9 August 2014. The peak ebb and flood are represented by blue and red circles, respectively.

We now consider simulations with turbines. Figure 10a,b shows the temporal evolution of the energy production per row for an aligned and a staggered layout. This figure highlights the great differences in production between the different rows, especially at peak ebb and flood. At those moments of the tide, the production of the upstream line (red curves) is greater than the production of the other rows because it is located in the free stream. For instance, the production of the second row (0.75 MW) is 34% smaller than the one of the first row (1.14 MW) for the aligned configuration without blockage corrections. When blockage corrections are included, the production of the second row (0.761 MW) is 35% lower than the production of the first row (1.19 MW). Figure 11 shows the time-averaged production of turbine per row. Regardless of the row, this figure shows that (1) the production of the staggered layout is greater than the one of the aligned layout and that (2) the production is greater when blockage corrections are included. For the staggered configuration, the difference in production between the first two rows is reduced. Whether

blockage correction is considered or not, the difference is about 4% between the two first rows (Figure 11). Averaging the production over the five rows, the blockage corrections increase the power output of the turbines by 3%, whether an aligned or staggered arrangement is considered. When including corrections, the production increases from 0.503 to 0.518 MW for the staggered layout and from 0.429 to 0.442 MW for the aligned turbines.

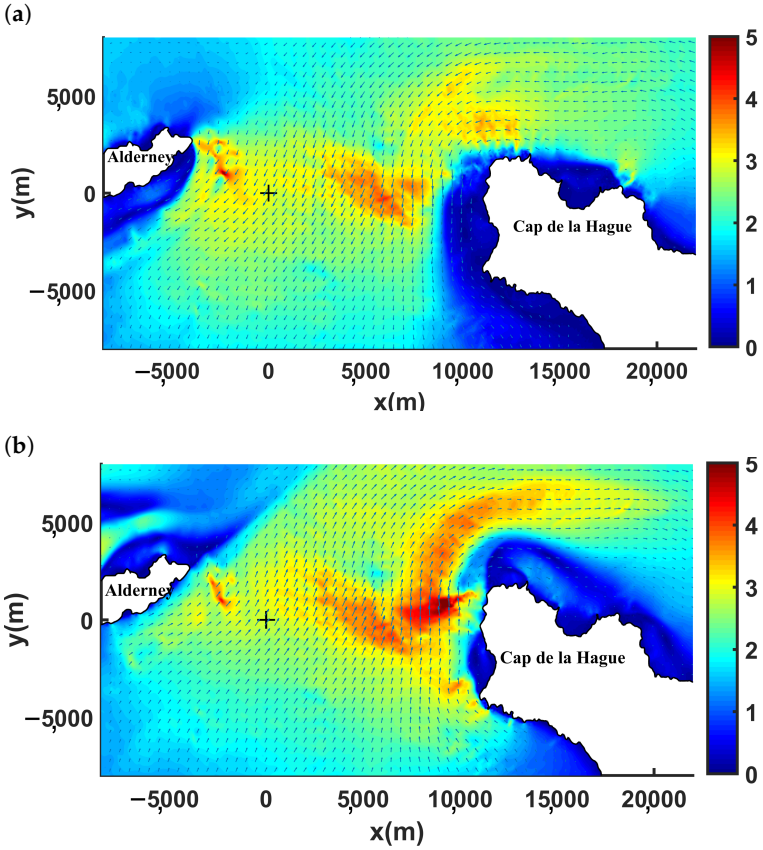

Figure 9. Spatial distribution of depth-averaged velocities (m/s) at (**a**) peak ebb and (**b**) flood during a mean spring tide in the Alderney Race (simulation without turbines). The cross represents the centre of the tidal farm. The origin of the reference frame (coordinates in m) corresponds to the centre of the farm.

We now investigate the factors controlling the change of turbine production induced by blockage corrections. To this end, we discriminate the effects of thrust and power corrections. Regarding the thrust, the correction tends to increase the momentum extraction, which has a direct impact on the wake-field. Thus, the effect of the thrust correction will be investigated by focusing on the changes of flow field (and hence the available power within the tidal farm) at both the array and the turbine scales. Regarding the power, the blockage correction is applied, as a second step, when assessing the power output with (Equation (22)), once the flow field has been computed. As the power correction has no influence on the flow field, its effect can, therefore, be easily discriminated from the effect of the thrust correction (which modifies the flow field). Thus, the effect of power correction is assessed, in a second step, by comparing (for a given flow field) the turbine output obtained with and without power correction.

Figure 12a shows the changes in the velocity magnitude induced by the thrust correction for an aligned turbine arrangement (difference between simulation with blockage corrections and without blockage corrections). Figure 12b shows the same difference for the staggered layout. The thrust correction induces, in both cases, a zone of deceleration upstream of the tidal farm (in blue) and restricts the velocity reduction on the sides of the array (in red). The deceleration is about 0.02 m/s upstream of the tidal farm (velocity

differences extracted 5D upstream of the tidal farm). Those changes of velocity distribution at the array-scale indicate that the blockage correction reinforces the flow bypasses around the tidal farm. This increased flow diversion leads to a slight loss of production as a decrease of 0.02 m/s corresponds to a reduction of current speed of 0.7% and a reduction of available power of 2%. However, the effect of the thrust correction appears more significant at the turbine scale. Indeed, immediately downstream the first row of turbines, the velocity reduction caused by the blockage reaches 0.10 m/s. This velocity reduction dissipates gradually in the longitudinal direction with different patterns for the staggered and the aligned layout, which explains the differences in the blockage effect between the rows. This reduction is due to the increase in thrust, which corresponds to a greater energy extraction. There is also a slight fluid acceleration caused by the blockage at the turbine scale, especially between the turbines of the first row. This is beneficial for the array production as the fluid acceleration results in a gain of production for the downstream turbines, especially for the staggered configurations.

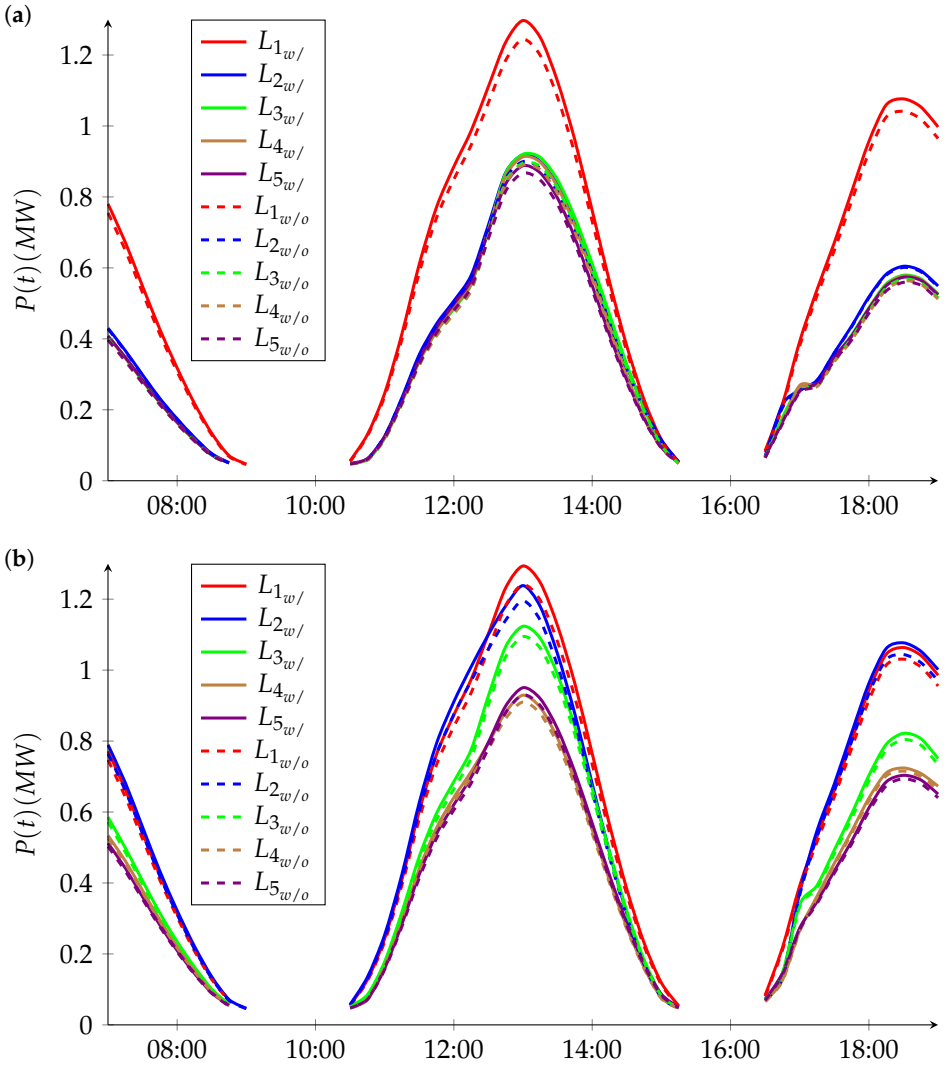

Figure 10. Time-series of output per row of turbines with (solid lines, curves captioned "w/") and without blockage corrections (dotted lines, curves captioned "w/o"). (**a**) Aligned and (**b**) staggered layouts. Note that rows/lines of turbines are ordered with respect to the incoming flow. Thus, line 1 refers to the line of devices facing the ebb and peak flow whereas line 5 refers to the last line of the turbine array.

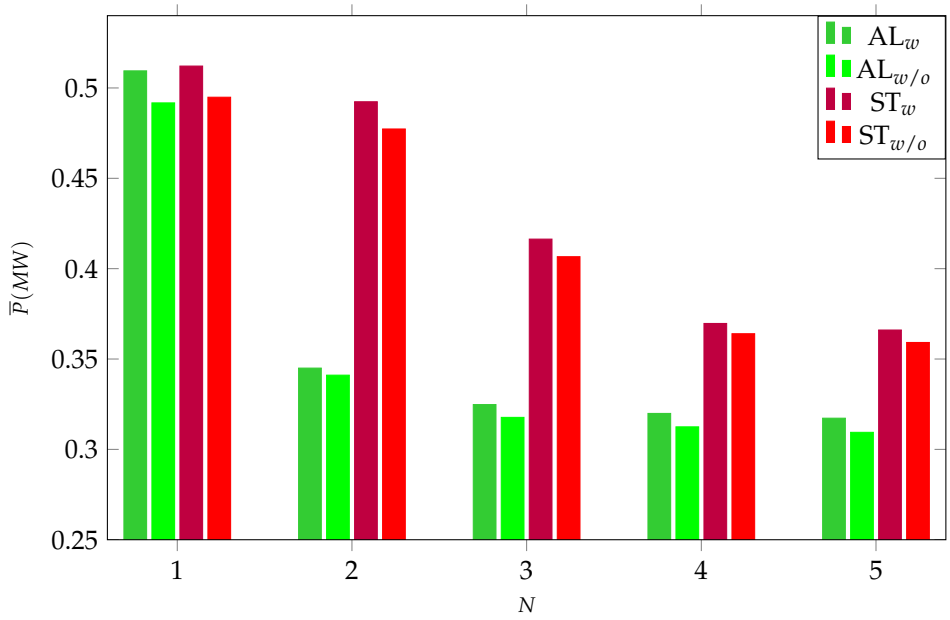

Figure 11. The mean production per row. The numbers of rows is N. For the aligned configuration, the lime green bar (AL$_w$) corresponds to the case with blockage correction and the green bar (AL$_{w/o}$) to the case without blockage correction. For the staggered configuration, the purple bar (ST$_w$) corresponds to the case with blockage correction and the red bar (ST$_{w/o}$) to the case without blockage correction.

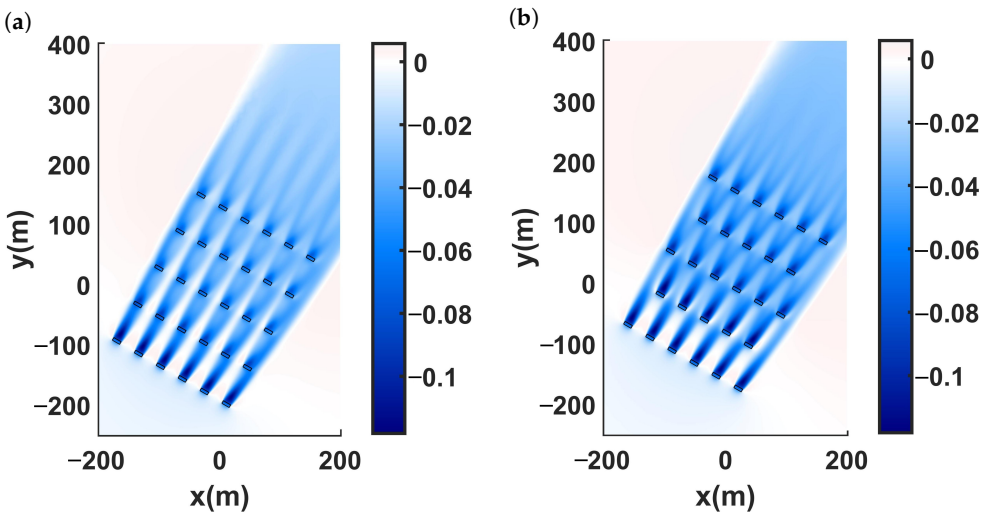

Figure 12. (**a**) Aligned arrangement and (**b**) staggered arrangement: difference in velocity magnitude with and without blockage corrections (in m/s). The results were extracted along a horizontal plane (located at the hub height) at peak flood of a mean spring tidal cycle (the seabed is quasi-horizontal).

Blockage corrections are, thus, found to have a noticeable effect on the velocity field within the tidal farm and, therefore, impact the turbine production. These effects are mainly characterised by a slowing down of the velocities (and thus a decrease in production). In our application, the decrease of production induced by the thrust correction is estimated at 11% for both the aligned and the staggered layouts. This value corresponds to the decrease in the cubed velocity (by comparing simulations with and without corrections). However, this decrease in production is counterbalanced by the increase of the power coefficient. The time–mean increase of production due to the correction of the resistance coefficient K (hence, the production) is 16% (for the two configurations). These counterbalanced effects result in a slight increase, of 3%, in the array production over a mean spring tidal cycle.

The efficiency of tidal farms is subjected to both turbines–wake interactions and by-pass flow accelerations. In this study, we aimed to understand the impact of blockage corrections on two different layouts (aligned and staggered). In line with [45], we found that the staggered layout had a greater efficiency than the aligned layout, whether a blockage correction was considered or not.

When blockage correction is included, the thrust is reinforced, which favours the flow deceleration through the turbine(s) and increases the by-pass flow-acceleration at both the turbine- and the array-scales. For realistic values of B ($B < 20\%$), comparable perturbations of the flow pattern (and associated loss of power) have been reported when the thrust increases [10,32]. It is, however, difficult to inter-compare quantitatively those studies as flow configurations and turbine settings are different from one study to another.

The perturbation of the flow field induced by the thrust correction is relatively small (of the order of 0.1 m/s). It is, thus, important to know if it is significant or not. In terms of power, the loss induced by the flow reduction is of the order of 11%, which is far from being negligible. Of note, such a velocity reduction is expected to have implications on other aspects, such as sediment transport and/or other geochemical processes that are functions of a higher power of the velocity magnitude [6,46,47]. Thus, blockage corrections need to be considered when assessing the impact of tidal-stream turbines on the environment.

Our results are, however, subject to several limitations. First, the Telemac3D model with actuator disks has been validated with laboratory measurements in the wake of a scaled turbine [4]. It is, therefore, important to bear in mind that, for operational applications, a model validation relying on measurements acquired in the wake of a full-scale turbine deployed in real sea conditions would be required. Unfortunately, such a dataset is not publicly available for the Alderney Race. Secondly, the LMADT relies on a simplified flow around the turbine. In particular, it neglects the rotation of the blades and the turbulent mixing in the wake. Furthermore, the LMADT is based on the assumption that power is the product of thrust and stream-wise flow through the rotor whereas, in practise, the power is equal to the torque multiplied by the rotor angular velocity. The values of the thrust and power corrections are, thus, subjected to uncertainties [48], especially for realistic applications where no proper validation exists due to the sparsity of measured data of thrust and power acquired on sites. Finally, our simulations focus on two extraction scenarios and results obtained are liable to vary with different array layouts. Furthermore, only the mean spring tide conditions were considered. Additional simulations with wider ranges of flow conditions and tidal farm characteristics (number of turbines, turbine diameter…) are required to generalise the results on the influence of the blockage corrections.

4. Conclusions

To improve the implementation of actuator disks in regional models, we proposed a method to integrate blockage corrections. The calculation of the thrust and power corrections rely on the model of Whelan et al. We investigated the impact of blockage corrections focusing on real-life scenarios of tidal stream energy extraction simulated with Telemac3D. The results showed that correcting the thrust favours the bypassing of the farm by the currents, which leads to a negligible loss of production. The correction of the thrust coefficient also tends to slow down the current velocities within the tidal farm due to the greater energy captured by the turbines and to create local zones of fluid acceleration, especially between the turbines of the upstream row. The thrust correction reduces the production by 11%. Despite this reduction in output, the overall production was slightly higher when blockage corrections were considered (about +3% in the tested cases), which is due to the increase of the power coefficient (of the order of 16%). This study, therefore, confirms that the performance of tidal turbines may be affected by the level of blockage. We also demonstrated that the blockage corrections should be integrated when assessing the annual energy production with numerical simulations. Moreover, as blockage corrections modify the velocity field in the tidal farm, they should also be considered when assessing the impact of tidal turbines on the physical environment.

Author Contributions: N.D.D.: Conceptualization, Methodology, Software, Formal analysis, Investigation, Writing—original draft. J.T.: Conceptualization, Methodology, Investigation, Writing—review and editing. S.G.: Conceptualization, Methodology, Investigation, Writing—review and editing. N.G.: Conceptualization, Methodology, Investigation, Writing—review and editing. All authors have read and agreed to the published version of the manuscript.

Funding: The PhD thesis of Nasteho Djama Dirieh is supported by Région Normandie. Jérôme Thiébot and Sylvain Guillou acknowledge the Interreg VA France (Channel) England Programme, which funds the TIGER project. The present paper is a contribution to the research program DI-ADEME ("Design et InterActions des Dispositifs d'extraction d'Energies Marines avec l'Environnement") of the Laboratory of Coastal Engineering and Environment (Cerema, http://www.cerema.fr, accessed on 9 May 2022).

Institutional Review Board Statement: Not applicable.

Informed Consent Statement: Not applicable.

Data Availability Statement: Not applicable.

Acknowledgments: The authors are grateful to the CRIANN for their help in using their computational resource and to the French navy SHOM ("Service Hydrographique et Océanographique de la Marine") for providing access to bathymetric (HOMONIM project) and sedimentological data (http://data.shom.fr/, accessed on 9 May 2022).

Conflicts of Interest: The authors declare no conflict of interest. The funders had no role in the design of the study; in the collection, analyses, or interpretation of data; in the writing of the manuscript, or in the decision to publish the results.

Abbreviations

The following abbreviations are used in this manuscript:

α	Ratio of the downstream to the upstream velocity, dimensionless
β	Ratio of the velocity in the disc to the upstream velocity, dimensionless
γ	Bypass induction factor, dimensionless
ε	Blockage ratio, dimensionless
ρ	Water density, kg/m^3
ν_{eff}	Effective kinematic viscosity, m^2 s^{-1}
δp	Pressure drop across the disc, kg m^{-1} s^{-2}
δz	Free surface elevation, m
A	Area swept by the blades, m^2
a	Axial induction factor,dimensionless
C_T	Thrust coefficient, dimensionless
C_P	Power coefficient, dimensionless
e	Thickness of the disc, m
F	Thrust force, kg m s^{-2}
Fr	Froude number, dimensionless
g	Acceleration of the earth's gravity, m/s^2
h	Water depth, m
K	Resistance coefficient, dimensionless
l	Transverse width of the flow, m
P_a	Atmospheric pressure, kg m^{-1} s^{-2}
s_1	Upstream area of the actuator disk per unit transverse width of the flow, m
s_d	Area of the actuator disk per unit transverse width of the flow, m
s_w	Far downstream area of the actuator disk per unit transverse width of the flow, m
S_x,S_y,S_z	Source terms, kg m^{-2}s^{-2}
t	Time, s
U_∞	Upstream velocity, m s^{-1}

U_d	Velocity in the disc, m s^{-1}
U_2	Velocity in the far downstream, m s^{-1}
U_w	Velocity in the far wake, m s^{-1}
u,v,w	Three components of the velocity, m s^{-1}
z_2	Water depth, m

References

1. Myers, L.; Bahaj, A. Simulated electrical power potential harnessed by marine current turbine arrays in the Alderney Race. *Renew. Energy* **2005**, *30*, 1713–1731. [CrossRef]
2. Myers, L.E.; Bahaj, A.S. An experimental investigation simulating flow effects in first generation marine current energy converter arrays. *Renew. Energy* **2012**, *37*, 28–36. [CrossRef]
3. Roc, T.; Conley, D.C.; Greaves, D. Methodology for tidal turbine representation in ocean circulation model. *Renew. Energy* **2013**, *51*, 448–464. [CrossRef]
4. Thiébot, J.; Guillou, S.; Nguyen, V.T. Modelling the effect of large arrays of tidal turbines with depth-averaged Actuator Disks. *Ocean Eng.* **2016**, *126*, 265–275. [CrossRef]
5. Olczak, A.; Stallard, T.; Feng, T.; Stansby, P.K. Comparison of a RANS blade element model for tidal turbine arrays with laboratory scale measurements of wake velocity and rotor thrust. *J. Fluids Struct.* **2016**, *64*, 87–106. [CrossRef]
6. Nash, S.; Phoenix, A. A review of the current understanding of the hydro-environmental impacts of energy removal by tidal turbines. *Renew. Sustain. Energy Rev.* **2017**, *80*, 648–662. [CrossRef]
7. Plew, D.R.; Stevens, C.L. Numerical modelling of the effect of turbines on currents in a tidal channel—Tory Channel, New Zealand. *Renew. Energy* **2013**, *57*, 269–282. [CrossRef]
8. Neill, S.P.; Jordan, J.R.; Couch, S.J. Impact of tidal energy converter (TEC) arrays on the dynamics of headland sand banks. *Renew. Energy* **2012**, *37*, 387–397. [CrossRef]
9. Guillou, N.; Chapalain, G.; Neill, S.P. The influence of waves on the tidal kinetic energy resource at a tidal stream energy site. *Appl. Energy* **2016**, *180*, 402–415. [CrossRef]
10. Houlsby, G.T.; Draper, S.; Oldfield, M.L.G. *Application of Linear Momentum Actuator Disc Theory to Open Channel Flow*; OUEL: Yao, Japan, 2008.
11. Draper, S.; Houlsby, G.; Oldfield, M.; Borthwick, A. Modelling tidal energy extraction in a depth-averaged coastal domain. *Renew. Power Gener. IET* **2010**, *4*, 545–554. [CrossRef]
12. Adcock, T.A.A.; Draper, S.; Houlsby, G.T.; Borthwick, A.G.L.; Serhadlıoğlu, S. The available power from tidal stream turbines in the Pentland Firth. *Proc. R. Soc. A Math. Phys. Eng. Sci.* **2013**, *469*, 20130072. [CrossRef]
13. Serhadlıoğlu, S.; Adcock, T.A.A.; Houlsby, G.T.; Draper, S.; Borthwick, A.G.L. Tidal stream energy resource assessment of the Anglesey Skerries. *Int. J. Mar. Energy* **2013**, *3–4*, e98–e111. [CrossRef]
14. Harrison, M.E.; Batten, W.M.J.; Myers, L.E.; Bahaj, A.S. Comparison between CFD simulations and experiments for predicting the far wake of horizontal axis tidal turbines. *IET Renew. Power Gener.* **2010**, *4*, 613–627. [CrossRef]
15. Abolghasemi, M.A.; Piggott, M.D.; Spinneken, J.; Viré, A.; Cotter, C.J.; Crammond, S. Simulating tidal turbines with multi-scale mesh optimisation techniques. *J. Fluids Struct.* **2016**, *66*, 69–90. [CrossRef]
16. Malki, R.; Masters, I.; Williams, A.J.; Nick Croft, T. Planning tidal stream turbine array layouts using a coupled blade element momentum—Computational fluid dynamics model. *Renew. Energy* **2014**, *63*, 46–54. [CrossRef]
17. Stallard, T.; Collings, R.; Feng, T.; Whelan, J. Interactions between tidal turbine wakes: Experimental study of a group of three-bladed rotors. *Philos. Trans. R. Soc. A Math. Phys. Eng. Sci.* **2013**, *371*, 20120159. [CrossRef]
18. Thiébot, J.; Guillou, N.; Guillou, S.; Good, A.; Lewis, M. Wake field study of tidal turbines under realistic flow conditions. *Renew. Energy* **2020**, *151*, 1196–1208. [CrossRef]
19. Michelet, N.; Guillou, N.; Chapalain, G.; Thiébot, J.; Guillou, S.; Goward Brown, A.J.; Neill, S.P. Three-dimensional modelling of turbine wake interactions at a tidal stream energy site. *Appl. Ocean Res.* **2020**, *95*, 102009. [CrossRef]
20. Nguyen, V.T.; Santa Cruz, A.; Guillou, S.S.; Shiekh Elsouk, M.N.; Thiébot, J. Effects of the Current Direction on the Energy Production of a Tidal Farm: The Case of Raz Blanchard (France). *Energies* **2019**, *12*, 2478. [CrossRef]
21. Abolghasemi, M.A.; Piggott, M.D.; Kramer, S.C. An investigation into the accuracy of the depth-averaging used in tidal turbine array optimisation. *arXiv* **2018**, arXiv:1810.09827.
22. McTavish, S.; Feszty, D.; Nitzsche, F. An experimental and computational assessment of blockage effects on wind turbine wake development. *Wind Energy* **2014**, *17*, 1515–1529. [CrossRef]
23. Bahaj, A.S.; Batten, W.M.J.; McCann, G. Experimental verifications of numerical predictions for the hydrodynamic performance of horizontal axis marine current turbines. *Renew. Energy* **2007**, *32*, 2479–2490. [CrossRef]
24. Nishino, T.; Willden, R.H.J. Effects of 3-D channel blockage and turbulent wake mixing on the limit of power extraction by tidal turbines. *Int. J. Heat Fluid Flow* **2012**, *37*, 123–135. [CrossRef]
25. Kinsey, T.; Dumas, G. Impact of channel blockage on the performance of axial and cross-flow hydrokinetic turbines. *Renew. Energy* **2017**, *103*, 239–254. [CrossRef]
26. Kolekar, N.; Vinod, A.; Banerjee, A. On Blockage Effects for a Tidal Turbine in Free Surface Proximity. *Energies* **2019**, *12*, 3325. [CrossRef]

27. Garrett, C.; Cummins, P. The efficiency of a turbine in a tidal channel. *J. Fluid Mech.* **2007**, *588*, 243–251. [CrossRef]
28. Whelan, J.I.; Graham, J.M.R.; Peiró, J. A free-surface and blockage correction for tidal turbines. *J. Fluid Mech.* **2009**, *624*, 281–291. [CrossRef]
29. Nishino, T.; Willden, R.H.J. The efficiency of an array of tidal turbines partially blocking a wide channel. *J. Fluid Mech.* **2012**, *708*, 596–606. [CrossRef]
30. Vogel, C.R.; Houlsby, G.T.; Willden, R.H.J. Effect of free surface deformation on the extractable power of a finite width turbine array. *Renew. Energy* **2016**, *88*, 317–324. [CrossRef]
31. Schluntz, J.; Willden, R.H.J. The effect of blockage on tidal turbine rotor design and performance. *Renew. Energy* **2015**, *81*, 432–441. [CrossRef]
32. Flores Mateos, L.; Hartnett, M. Hydrodynamic Effects of Tidal-Stream Power Extraction for Varying Turbine Operating Conditions. *Energies* **2020**, *13*, 3240. [CrossRef]
33. Thiébot, J.; Djama Dirieh, N.; Guillou, S.; Guillou, N. The Efficiency of a Fence of Tidal Turbines in the Alderney Race: Comparison between Analytical and Numerical Models. *Energies* **2021**, *14*, 892. [CrossRef]
34. Campbell, R.; Martinez, A.; Letetrel, C.; Rio, A. Methodology for estimating the French tidal current energy resource. *Int. J. Mar. Energy* **2017**, *19*, 256–271. [CrossRef]
35. Coles, D.S.; Blunden, L.S.; Bahaj, A.S. Assessment of the energy extraction potential at tidal sites around the Channel Islands. *Energy* **2017**, *124*, 171–186. [CrossRef]
36. Bailly du Bois, P.; Dumas, F.; Morillon, M.; Furgerot, L.; Voiseux, C.; Poizot, E.; Méar, Y.; Bennis, A.C. The Alderney Race: General hydrodynamic and particular features. *Philos. Trans. R. Soc. A Math. Phys. Eng. Sci.* **2020**, *378*, 20190492. [CrossRef]
37. Guillou, N.; Neill, S.P.; Thiébot, J. Spatio-temporal variability of tidal-stream energy in north-western Europe. *Philos. Trans. R. Soc. A Math. Phys. Eng. Sci.* **2020**, *378*, 20190493. [CrossRef]
38. Sentchev, A.; Nguyen, T.D.; Furgerot, L.; Bailly du Bois, P. Underway velocity measurements in the Alderney Race: Towards a three-dimensional representation of tidal motions. *Philos. Trans. R. Soc. A Math. Phys. Eng. Sci.* **2020**, *378*, 20190491. [CrossRef]
39. Thiébot, J.; Coles, D.S.; Bennis, A.C.; Guillou, N.; Neill, S.; Guillou, S.; Piggott, M. Numerical modelling of hydrodynamics and tidal energy extraction in the Alderney Race: A review. *Philos. Trans. R. Soc. A Math. Phys. Eng. Sci.* **2020**, *378*, 20190498. [CrossRef]
40. Lo Brutto, O.A.; Nguyen, V.T.; Guillou, S.S.; Thiébot, J.; Gualous, H. Tidal farm analysis using an analytical model for the flow velocity prediction in the wake of a tidal turbine with small diameter to depth ratio. *Renew. Energy* **2016**, *99*, 347–359. [CrossRef]
41. Hervouet, J.M. *Hydrodynamics of Free Surface Flows: Modelling with the Finite Element Method*; John Wiley & Sons: Hoboken, NJ, USA, 2007. [CrossRef]
42. Kramer, S.C.; Piggott, M.D. A correction to the enhanced bottom drag parameterisation of tidal turbines. *Renew. Energy* **2016**, *92*, 385–396. [CrossRef]
43. Taylor, G.I. *The Scientific Papers of Sir Geoffrey Ingram Taylor: Mechanics of Solids*; CUP Archive; Cambridge University Press: Cambridge, UK, 1958; Volume 1.
44. Bahaj, A.S.; Molland, A.F.; Chaplin, J.R.; Batten, W.M.J. Power and thrust measurements of marine current turbines under various hydrodynamic flow conditions in a cavitation tunnel and a towing tank. *Renew. Energy* **2007**, *32*, 407–426. [CrossRef]
45. Ouro, P.; Nishino, T. Performance and wake characteristics of tidal turbines in an infinitely large array. *J. Fluid Mech.* **2021**, *925*. [CrossRef]
46. Adcock, T.A.A.; Draper, S.; Nishino, T. Tidal power generation—A review of hydrodynamic modelling. *Proc. Inst. Mech. Eng. Part A J. Power Energy* **2015**, *229*, 755–771. [CrossRef]
47. Bonar, P.A.J.; Bryden, I.G.; Borthwick, A.G.L. Social and ecological impacts of marine energy development. *Renew. Sustain. Energy Rev.* **2015**, *47*, 486–495. [CrossRef]
48. Ross, H.; Polagye, B. An experimental assessment of analytical blockage corrections for turbines. *Renew. Energy* **2020**, *152*, 1328–1341. [CrossRef]